Since January 2020 Elsevier has created a COVID-19 resource centre with free information in English and Mandarin on the novel coronavirus COVID-19. The COVID-19 resource centre is hosted on Elsevier Connect, the company's public news and information website.

Biochemical Pharmacology 188 (2021) 114564

Contents lists available at ScienceDirect

Biochemical Pharmacology

journal homepage: www.elsevier.com/locate/biochempharm

Discovery of a AHR pelargonidin agonist that counter-regulates Ace2 expression and attenuates ACE2-SARS-CoV-2 interaction

Michele Biagioli [a], Silvia Marchianò [a], Rosalinda Roselli [b], Cristina Di Giorgio [a], Rachele Bellini [a], Martina Bordoni [a], Anna Gidari [a], Samuele Sabbatini [a], Daniela Francisci [a], Bianca Fiorillo [b], Bruno Catalanotti [b], Eleonora Distrutti [c], Adriana Carino [a], Angela Zampella [b], Gabriele Costantino [d], Stefano Fiorucci [a,*]

[a] Dipartimento di Medicina e Chirurgia, Università di Perugia, Perugia, Italy
[b] University of Naples Federico II, Department of Pharmacy, Naples, Italy
[c] SC di Gastroenterologia ed Epatologia, Azienda Ospedaliera di Perugia, Perugia, Italy
[d] Department of Food and Drugs, University of Parma, Parma, Italy

ARTICLE INFO

Keywords:
Pelargonidin
Intestinal inflammation
TNF-α
Ahr
ACE2
NF-kB
SARS-CoV-2

ABSTRACT

The severe acute respiratory syndrome (SARS)-CoV-2 is the pathogenetic agent of Corona Virus Induced Disease (COVID)19. The virus enters the human cells after binding to the angiotensin converting enzyme (ACE)2 receptor in target tissues. *ACE2* expression is induced in response to inflammation. The colon expression of *ACE2* is upregulated in patients with inflammatory bowel disease (IBD), highlighting a potential risk of intestinal inflammation in promoting viral entry in the human body. Because mechanisms that regulate *ACE2* expression in the intestine are poorly understood and there is a need of anti-SARS-CoV-2 therapies, we have settled to investigate whether natural flavonoids might regulate the expression of *Ace2* in intestinal models of inflammation. The results of these studies demonstrated that pelargonidin activates the Aryl hydrocarbon Receptor (AHR) *in vitro* and reverses intestinal inflammation caused by chronic exposure to high fat diet or to the intestinal braking-barrier agent TNBS in a AhR-dependent manner. In these two models, development of colon inflammation associated with upregulation of *Ace2* mRNA expression. Colon levels of *Ace2* mRNA were directly correlated with *Tnf-α* mRNA levels. Molecular docking studies suggested that pelargonidin binds a fatty acid binding pocket on the receptor binding domain of SARS-CoV-2 Spike protein. *In vitro* studies demonstrated that pelargonidin significantly reduces the binding of SARS-CoV-2 Spike protein to ACE2 and reduces the SARS-CoV-2 replication in a concentration-dependent manner. In summary, we have provided evidence that a natural flavonoid might hold potential in reducing intestinal inflammation and *ACE2* induction in the inflamed colon in a AhR-dependent manner.

1. Introduction

The coronavirus disease 2019 (COVID-19) is a respiratory tract infection caused severe acute respiratory syndrome (SARS)-CoV-2, a newly emerged coronavirus first identified in the city of Wuhan in China in December 2019 [1]. The SARS-CoV2 virus entry into host cells is mediated by interaction between the spike (S) glycoprotein, that assembly into an homotrimeric complex protruding from the viral surface, with the angiotensin-converting enzyme 2 (ACE2) [2]. The spike glycoprotein comprises two functional subunits: the S1 subunit contains a specific motif, the receptor-binding domain (RBD), that is responsible for binding to ACE2, while the S2 subunit is essential for fusion of the viral and cellular membranes [2] Thus, targeting the interaction of spike's RBD with ACE2 might hold potential for the treatment of COVID 19. Accordingly, several agents that target the SARS-CoV2/ACE2 interaction, including several monoclonal antibodies, have been identified and tested clinically. Following a similar approach, it has been suggested that modulation of *ACE2* expression could also be of interest in reducing SARS-CoV2 entry in target cells [2–7].

The expression of *ACE2* vary greatly among human tissues. In the normal lung, *ACE2* mRNA is mainly expressed by type I and II alveolar (AT1 and AT2) epithelial cells and endothelial cells [8,9]. However, it

* Corresponding author.
E-mail address: stefano.fiorucci@unipg.it (S. Fiorucci).

https://doi.org/10.1016/j.bcp.2021.114564
Received 12 March 2021; Received in revised form 9 April 2021; Accepted 12 April 2021
Available online 17 April 2021

has been shown that the expression of *ACE2* in the lung increases in response to inflammation or exposure to interferon IFN-γ [10]. In normal individual, *ACE2* mRNA and protein are highly expressed in the gastrointestinal system, in particular in the duodenum, jejunum, ileum, and colon, although the functional role of this peptidase in intestinal epithelial cells remains portly elucidated [11]. Furthermore, similarly to the lung, the intestinal expression of *ACE2* is modulated in response to intestinal inflammation in inflammatory bowel disease (IBD) in a phenotype dependent manner [12]. More specifically, while expression of *ACE2* is reduced in the ileum of patients with active Crohn disease, an elevated colonic expression of *ACE2* mRNA has been reported in ulcerative colitis patients with active inflammation and severe disease [13–15]. Since the colonic *ACE2* levels normalize after anti-cytokine therapy and the anti-cytokine therapy associates with reduced morbidity of IBD patients from COVID19, these data establish a relation between the levels of colonic *ACE2* expression and beneficial effects exerts by anti-cytokine therapies. Moreover, the evaluation of SECURE-IBD registry (available http://www.covidibd.org) suggest that patients with IBD are under-represented in those diagnosed with COVID-19 compared to the general populations [16]. Despite these data raise interest on ACE2 as potential target in IBD in the frame of COVID19 pandemia, the mechanisms involved in *ACE2* regulation in the intestine are only partially understood. Further on, it is unclear whether *ACE2* expression could be modulated with dietary factors that might have also utility in reducing inflammation.

The aryl hydrocarbon receptor (AhR) is a ligand-activated transcription factor that belongs to the basic helix-loop-helix (bHLH)/Per-ARNT-Sim (PAS) superfamily. Although AHR was originally described as a xenobiotics sensor, it is now well established that dietary/intestinal microbiota metabolites represent the physiological ligands [17]. Similarly, to other nuclear receptors, in the absence of a ligand, AHR resides in cytoplasm as a component of a chaperone complex [18]. The *AhR* is widely expressed by cells of innate/adaptive immunity [19] but it is also expressed at high levels by intestinal epithelial cells where it is essential for maintaining the integrity of the intestinal barrier and therefore for regulating the inflammatory state of the gastrointestinal tract [20,21].

Pelargonidin is a water soluble anthocyanidin that is widely diffuse in nature as glycosylated derivatives and that is responsible for the red/orange colours of berries such as raspberries and strawberries, as well as blueberries and blackberries [22]. While, similarly to other anthocyanins, pelargonidin is thought to be beneficial for human health [23–25], controversies exist over the doses needed to reach these effects, along with poor systemic bioavailability and unclear mechanism(s) of action. In a previous study we have shown that the natural pelargonidin function as AHR ligand *in vitro* and attenuates intestinal inflammation in AHR-dependent manner [26]. In the present study we have investigated the potential of the natural pelargonidin in regulating *Ace2* expression in colon in models of intestinal inflammation caused by exposure of wild type and $AhR^{-/-}$ mice to a high caloric intake and intestinal irritants. The results of these studies show that not only a dietary agent might regulate the expression of the *Ace2* in the colon but also inhibit the interaction of SARS-CoV2′s spike protein with ACE2, providing a potentially useful clues in the prevention and treatment of COVID19.

2. Material and methods

2.1. Transactivation assay

For AhR-mediated transactivation, HepG2 cells were plated at 7.5×10^4 cells/well in a 24-well plate. Cells were transiently transfected with 200 ng of the reporter vector pLightAhRE, 100 ng of pCMVXL4AhR, and 100 ng of pGL4.70 (Promega, Madison, WI, USA), a vector encoding the human *RENILLA* luciferase gene. At 24 h post-transfection, cells were stimulated 18 h with Pelargonidin 10 and 50 μM (Merk Group, Darmstadt, GE). Dose-response curves were performed in HepG2 cells transfected with *AHR*, as described above, and then treated with increasing concentrations of Pelargonidin (1, 2.5 5, 10, 12.5, 25, 50, 75, 100 μM).

At 18 h post-stimulation, cellular lysates were assayed for luciferase and RENILLA activities using the Dual-Luciferase Reporter assay system (Promega, Madison, WI, USA). Luminescence was measured using Glomax 20/20 luminometer (Promega, Madison, WI, USA). LUCIFERASE activities (RLU) were normalized with RENILLA activities (RRU).

2.2. Mouse spleen macrophages purification

Spleens were collected from $AhR^{+/+}$ and $AhR^{-/-}$ mice. Spleens were homogenized and then red blood cell lysis was performed using a hypotonic solution. After cell count, the cell pellet was resuspended at a concentration of 10^8/ mL, to proceed to the positive selection of $Cd11b^+$ cells. In particularly, macrophages were purified using CD11b microbeads (Miltenyi Biotec, Bergisch Gladbach, GE), according to the manufacturer's instructions. Subsequently the selected macrophages have been plated at a concentration of 500.000/mL and were activated with LPS (5 ng/mL, Merk Group, Darmstadt, GE) in combination with IFN-γ (20 ng/mL, eBioscience, San Diego, CA, USA) for 16 h alone or in addition to Pelargonidin (20 μM) for gene expression profile analysis.

2.3. Animals

All animal care and experimental procedures complied with the guidelines of Animal Care and were approved by Use Committee of the University of Perugia and by the Italian Minister of Health and Istituto Superiore di Sanità (Italy) and was in agreement with the European guidelines for use of experimental animals (permissions n. 583/2017-PR and 1126/2016-PR). The general health conditions of the animals were monitored daily by the veterinarian in the animal facility. The study protocol caused minor suffering. However, mice with an hight grade of pain were eutanized. *AhR* knock out mice ($Ahr^{-/-}$) on C57BL/6 background and their C57BL/6 congenic littermates wild type ($Ahr^{+/+}$) were originally supplied by Charles River (Wilmington, MA, USA). Colonies were housed under controlled temperature (22 °C) and photoperiods of 12:12-h light/dark cycle in restricted access area and abled to acclimate to these conditions for at least 7 days before inclusion in an experiment.

To reproduce a mouse model of Acute Colitis a 2,4,6-trinitrobenzenesulfonic acid (Sigma Chemical Co, St Louis, MO) (TNBS)-colitis model is used as previously described [27]. Briefly, according to this 8–10 weeks old male mice C57BL/6J wild-type and $Ahr^{+/+}$ and $Ahr^{-/-}$ on C57BL/6J genetic background were administrated. Briefly, mice were fasted for 12 h overnight (Day −1). The next day (Day 0), mice were sedated by administration of Zoletil at a dose of 50 mg/Kg of body weight. Then a 3.5F = 11.55 mm catheter was inserted into the colon such that it was up to 4 cm from the anus and 1 mg of TNBS in 50% ethanol administered via the catheter into the colon lumen using a 1 mL syringe (injection volume of 100 μL). Control mice received 50% ethanol alone. Pelargonidins were administered by oral gavage (1, 5 or 10 mg/kg) daily from day 0 to the 4 day, that is the day of sacrifice. The severity of colitis was scored daily for each mouse by assessing body weight, the fecal occult blood, and stool consistency. Each parameter was scored from 0 to 4 and the sum represents the Colitis Disease Activity Index (CDAI). The scoring system was as follows: Percent of body weight loss: None = 0; 1–5% = 1; 5–10% = 2; 10–20% = 3; >20% = 4. Stool consistency: Normal = 0; soft but still formed = 1; very soft = 2; diarrhea = 3; liquid stools that stick to the anus or anal occlusion = 4. Fecal blood: None = 0; visible in the stool = 2; severe bleeding with fresh blood around the anus and very present in the stool = 4. On day 4, surviving mice were sacrificed, blood samples collected by facial vein, and the colon excised, measured length and weight, and evaluated for macroscopic damage.

To investigate the effects of Pelargonidins in a mouse model of NASH, 10–12 weeks old C57BL/6 male mice, *Ahr* wild type ($Ahr^{+/+}$) and their congenic littermates *AhR* null mice ($Ahr^{-/-}$) were fed a high fat diet containing 59 KJ% fat plus 1% cholesterol, w/o sugar (ssniff, Soest, GE) and fructose in drinking water (42 g/L) for 8 weeks as previously

described [28]. Food intake was valued as the difference of weight between the provided and the remnant amount of food at 2-day intervals. The food was provided as pressed pellets and the residual spillage was not considered. After 8 days, $Ahr^{+/+}$ and $Ahr^{-/-}$ HFD-F mice were randomized to receive HFD-F alone or plus Pelargonidin (5 mg/Kg/die) by oral gavage for remaining 7 weeks. On the sacrifice day, fed mice were deeply anesthetized with Zoletil at a dose of 50 mg/Kg and sacrificed before 12 AM. Thus, blood, liver, small intestine, colon, spleen, epididymal adipose tissue (eWAT), brown adipose tissue (BAT) and gastrocnemius were collected. The abdominal circumference (AC) (immediately anterior to the forefoot), body weight, and body length (nose-to-anus or nose–anus length), were measured in anaesthetized mice at the day of sacrifice. The body weight and body length were used to calculate the Body mass index (BMI) (=body weight (g)/length^2 (cm^2)).

2.4. Intestinal permeability

Intestinal permeability test was performed using fluorescein isothiocyanate conjugated dextran (FITC-dextran) (Sigma-Aldrich, St. Louis, MO, USA). FITC-dextran was dissolved in PBS at a concentration of 100 mg/mL. The evening before the test day mice were fasted overnight. In the next morning, after weighing each mouse, FITC was administered to each one at a dose of 44 mg/100 g of body weight by oral gavage. After 4 h, the mice were anesthetized by inhalation of isoflurane and 300–400 μL of blood collected from the facial vein in microtubes containing EDTA (Invitrogen, Carlsbad, CA, USA). Blood was stored in the dark. Once blood has been collected from all the mice, microtubes were processed to separate the serum. For analysis, serum was diluted with an equal volume of PBS (Euroclone S.p.a Milan, IT). The concentration of FITC in serum was determined by spectrophoto fluorometry with an excitation of 485 nm and an emission wavelength of 528 nm using as standard serially diluted FITC-dextran (0, 125, 250, 500, 1000, 2000, 4000, 6000, 8000 ng/ml). Serum from mice not administered with FITC-dextran was used to determine the background.

2.5. Histology

Colon sample (2–3 cm up anus) were first fixed in 10% Formalin (Bio-Optica Milano S.p.A. Milan, IT), embedded in Paraffin (Bio-Optica Milano S.p.A. Milan, IT), cut into 5-μm-thick sections and then stained with Hematoxylin/Eosin (H&E) (Bio-Optica Milano S.p.A. Milan, IT) for histopathological analysis. The histological score of the colon was assessed as previously described by U. Erben et al. [29]. This score evaluated the level of tissue inflammation in relation to the extension of the inflammatory cell infiltrate (mild severity if the cellular infiltrate is only present in the mucosa, moderate if they are involved mucosa and submucosa, marked if the infiltration is transmural), and epithelial changes of the intestinal mucosal architecture like erosions and ulcerations.

Immunohistochemistry was performed on paraffin embedded colon. In brief, Ag retrieval was achieved by incubation of the slides for 90 min in the hot (95 °C) sodium citrate buffer (pH 6.0) and 30 min of cooling at room temperature. Immunostaining technique was performed using the commercial kit Elabscience®2-step plus Poly-HRP Anti Rabbit/Mouse IgG Detection System (with DAB Solution) (Houston, Texas 77079, USA.) ACE2 Recombinant Rabbit Monoclonal Antibody (SN0754) Invitrogen, Thermofisher scientific (Waltham, Massachusetts, USA) was incubated overnight at 4C. Subsequently, sections were incubated with Polyperoxidase-anti-Mouse/Rabbit IgG and then with DAB Working Solution, both supplied by the kit. Slides were counterstained with hematoxylin, dehydrated through ethanol and xylene, and coverslipped using a xylene-based mounting medium.

2.6. Quantitative Real-Time PCR analysis

RNA was extracted from mouse colon and spleen macrophages using respectively TRIzol reagent (Invitrogen, Carlsbad, CA, USA) and Direct-zol™ RNA MiniPrep w/Zymo-Spin™ IIC Columns (Zymo Research, Irvine, CA, USA). 1 μg of RNA from each sample was reverse transcribed using FastGene Scriptase Basic Kit (Nippon Genetics Europe, Düren, GE) in a 20-μL reaction volume; 50 ng of cDNA was amplified in a 20-μL solution containing 200 nM of each primer and 10 μL of SYBR Select Master Mix (Thermo Fisher Scientific, Waltham, MA, USA). All reactions were performed in triplicate using the following thermal cycling conditions: 3 min at 95 °C, followed by 40 cycles of 95 °C for 15 s, 56 °C for 20 s, and 72 °C for 30 s, using a StepOnePlus system (Applied Biosystems, Foster City, CA, USA). The relative mRNA expression was calculated according to the ΔCt method. Primers were designed using the software PRIMER3 (http://frodo.wi.mit.edu/primer3/), using data published in the NCBI database. The primer used were as following (forward and reverse): *mGapdh* (for CTGAGTATGTCGTGGAGTCTAC; rev GTTGGTGGTGCAGGATGCATTG), *mTnfα* (for CCACCACGCTCTTCTGTCTA; rev AGGGTCTGGGCCATAGAACT), *mIl-6* (for CTTCACAAGTCGGAGGCTTA; rev TTCTGCAAGTGCATCATCGT), mTgfβ (for TTGCTTCAGCTCCACAGAGA; rev TGGTTGTAGAGGGCAAGGAC), *mAce2* (for AGATGGCCGGAAAGTTGTCT; rev GGGCTGTCAAGAAGTTGTCC), *mMas* (for CTGCTGACAGCCATCAGTGT; rev ACAGAAGGGCACAGACGAAT), *mIl1β* (for GCTGAAAGCTCTCCACCTCA; rev AGGCCACAGGTATTTTGTCG), *Cyp1a1* (for ACTCTTCCCTGGATGCCTTC; rev GTCTGTGATGTCCCGGATGT) (Thermo Fisher Scientific, Waltham, MA, USA).

2.7. Cell culture

Caco-2 cells, a human intestinal epithelial cell line (Sigma-Aldrich St. Louis, MO, USA) was grown at 37 °C in D-MEM (Euroclone S.p.a Milan, IT) containing 10% FBS (Euroclone S.p.a Milan, IT), 1% l-glutamine (Euroclone S.p.a Milan, IT), and 1% penicillin/streptomycin (Euroclone S.p.a Milan, IT). Cells were regularly passaged to maintain exponential growth. Caco-2 cells were classically activated with hTNF-α (Sino Biological, Beijing, CN) 100 ng/ml for 24 h alone or in combination with Pelargonidin (5, 10, and 20 μM) for the analysis of expression of several genes.

2.8. Mouse colon epithelial cells (IECs) purification and culture

Colon were collected from 6 to 10 weeks $Ahr^{+/+}$ and $Ahr^{-/-}$ mice. Organs were cleaned of feces by flushing with PBS 2% Fetal bovine serum (FBS) using a syringe and were cut first longitudinally and then laterally into 0.5 cm length pieces. Each tissue pieces were incubated for 30 min at 37 °C in 10 mL digestion solution containing DMEM with 5% FBS, 10 mM HEPES (Euroclone S.p.a Milan, IT), 5 mM EDTA, 1 mM DTT (Sigma-Aldrich, St. Louis, MO, USA). After incubation, samples were mixed for 30 s using a vortex mixer. Cell suspensions were stored on ice and supernatant were separate from colon tissue pieces and transferred into new tube after were applied into a MACS SmartStrainer 100 μm (Miltenyi Biotec, Bergisch Gladbach, GE) placed on a 15 mL tube. After centrifugation cell suspension were applied onto a MACS SmartStrainer 75 μm (Miltenyi Biotec, Bergisch Gladbach, GE) for remove impurity and resuspended in DMEM containing 10% FBS, 1% l-glutamine, and 1% penicillin/streptomycin.

Approximately 1×10^6 extracted cells were seeded in 24 well plate and incubated at 37 °C for 2 h. After incubation IEC cells were treated with mTNF-α (Sino Biological, Beijing, CN) 100 ng/mL for 20 h alone or in combination with Pelargonidin (5, 10, and 20 μM) and mNF-κB inhibitor (Sigma-Aldrich, St. Louis, MO, USA) 100 nM for gene expression profile analysis.

2.9. ACE2/SARS-CoV-2 Spike inhibitor Screening assay Kit

Pelargonidin at different concentrations (1–10-20–50 μM) was tested using the ACE2: SARS-CoV-2 Spike Inhibitor Screening Assay Kit (BPS Bioscience San Diego, CA, USA) according to the manufacturer's instructions. Briefly, we have thawed ACE2 protein on ice and diluted to 1 μg/ml in PBS. We have used 50 μL of ACE solution to coat a 96-well nickel-coated plate (1 h). The plate was washed 3 times and incubated for 10 min with a Blocking Buffer. Next, 10 μL of inhibitor solution containing the Pelargonidin was added to wells and incubated for 1 h at room temperature with slow shaking. For the "Positive Control" and "Blank," 10 μL of inhibitor buffer (5% DMSO, Sigma-Aldrich, St. Louis, MO, USA, solution) were used. After the incubation (1 h), SARS-CoV-2 SPIKE (RBD)-Fc was thawed on ice and diluted to 0.25 ng/μL (≈5 nM) in Assay Buffer 1; 5 nM SPIKE protein was added to each well, except to the blank. The reaction was incubated for 1 h at room temperature, with slow shaking. After 3 washes and incubation with a Blocking Buffer (10 min), we have treated the plate with an Anti-mouse-Fc-HRP and the plate was incubated for 1 h at room temperature with slow shaking. Finally, HRP substrate was added to the plate to produce chemiluminescence, which was measured using FluoStar Omega microplate reader (BMG LABTECH Ortenberg, GE).

To confirm the validity of the assay used in this study, remnants of plasma samples used to test levels of anti-SARS CoV2 IgG in post COVID-19 patients were used. The original samples were collected at the blood bank of Azienda Ospedaliera of Perugia from post COVID-19 donors who participate to a program of plasma biobanking. The program's protocol included the quantitative analysis of the anti-SARS-CoV-2 IgG antibodies directed against the subunits (S1) and (S2) of the virus SPIKE protein. An informed consent was obtained by each donor for the use of the plasma sample remnants and the protocol was approved by the Ethical Committee of the University of Perugia: authorization n. 61,843 (July 13,2020).

2.10. Virus isolation and cell cultures

The experiments were performed in Biological Safety Level 3 (BSL-3) virology laboratory of "Santa Maria della Misericordia" Hospital, Perugia, Italy. The SARS-CoV-2 strain was isolated as previously described [30]. For viral propagation, Vero E6 cell line was maintained in Eagle minimal essential medium (MEM) supplemented with 10% foetal bovine serum (FBS) and 100 U/mL penicillin–streptomycin solution. After isolation, SARS-CoV-2 titer was determined by Median Tissue Culture Infectious Dose (TCID50) endpoint dilution and stock aliquots were stored at −80 °C. The stock virus titer was 4.22×10^7 TCID50/mL.

2.11. SARS-CoV-2 yield reduction assay

Vero E6 cells (20,000 cells/well) were seeded in 96-well clear flat-bottom plates and incubated at 37 °C with 5% CO_2 for 24 h. After incubation, Pelargonidin at concentration of 20, 50 and 100 μM, and Remdesivir 10 μM (Veklury, Gilead, US) all diluted in complete medium were added to each well and then, cells were infected with SARS-CoV-2 (50 or 100 TCID50/well). Negative controls (pelargonidin or Remdesivir alone), infected positive controls (SARS-CoV-2 alone) and mock-infected cells were included in each plate. Plates were incubated at 37 °C with 5% CO_2 for 48 h. After the incubation, supernatants of 5 technical replicates were pooled and stored at −80 °C for further analysis.

2.12. Plaque-reduction assays

Supernatants viral titer was determined by plaque assay as previously described [31], with some modifications. Vero E6 cells (600,000 cells/well) were seeded in a 6-well plate and incubated at 37 °C with 5% CO_2 for 24 h. After incubation, the medium was removed and cells were infected with 500 μL of ten-fold serial dilution of supernatant previously obtained, rocking the plates every fifteen minutes. In the meanwhile, the overlay medium (complete medium with Agar 0.1%) was prepared and maintained in a 50 °C water bath. After 1 h of infection, the overlay medium (2 mL) was poured into each well and the plates incubated for 3 days. Finally, the overlay was discarded, cells were fixed for 30 min with 4% formalin and stained with 0.5% crystal violet. Viral titer was determined as plaque-forming units per mL, considering wells with plaques ranging from 2 to 100. For each pool of supernatants, plaque-reduction assay was performed in duplicate.

2.13. Computational studies

Two cryo-electron microscopy structures of SARS-CoV2 were employed for docking calculations, in the central b-sheet core and in the flavonoids binding pocket (PDB ID: 6VSB) [32], while for dockings in the fatty acids (FA) pocket we used the (PDB ID 6ZB5) [33]. The receptor was treated with the Protein Preparation [34] tool implemented in Maestro ver. 11.8. (Schrödinger Release 2019–1: Maestro, New York). The 3D structure of pelargonidin was built using the Graphical User Graphical User Interface (GUI) of Maestro ver. 11.8. (Schrödinger Release 2019–1: Maestro, New York). The protonation state of Pelargonidin at pH 7.4 in water has been calculated using the Epik module [35]. Finally, the compound was then minimized using the OPLS 2005 force field through 2500 iteration steps of the Polak-Ribiere Conjugate Gradient (PRCG) [36] algorithm.

The docking procedure was realized with the Glide software package (Glide, version 7.1. New York, NY: Schrödinger, LLC, 2019) using the Standard Precision (SP) algorithm of the GlideScore function [37] and the OPLS 2005 force field [38]. A grid box of 20 × 20 × 20 Å for SARS-CoV2 receptor centered on the putative binding pocket was created. A total amount of 100 poses was generated. Docking conformations of pelargonidin were then clustered based on their atomic RMSD and five clusters were obtained. Among them, only the conformation included in the most populated cluster with both the Glide Emodel and GlideScore-docking lowest-energy value was considered.

2.14. Statistical analysis

The two-tailed unpaired Student' s *t* test was used for statistical comparisons (*$P < 0.05$) using the Prism 6.0 software (GraphPad). The calculation of Person r, P value and R squared was performed in the correlation graphs using the Prism 6.0 software (GraphPad).

3. Results

3.1. Activity of the natural compounds toward AHR

We have first investigated whether the natural pelargonidin exerted agonistic effects on AHR. The activity of pelargonidin was evaluated in a Luciferase reporter assay using HepG2 cells, transiently transfected with a *AHR* reporter gene cloned upstream to the *LUCIFERASE*. HepG2 were incubated with 5 nM TCDD, an AHR agonist as a control, or vehicle (0.1% v/v DMSO) in the presence of the Pelargonidin (10–50 μM) for 18 h. As shown in Fig. 1A, Pelargonidin was found effective in transactivating the AHR; furthermore, in a concentration–response curve analysis, we found that pelargonidin transactivated AHR with a relative potency, expressed as EC50, of 12 μM (Fig. 1B).

3.2. Pelargonidin rescues from intestinal inflammation in TNBS-induced colitis in mice and restore Ace2 expression

We have investigated whether pelargonidin administration attenuates intestinal inflammation in a mouse model of colitis. We first performed a dose finding experiment by administering Pelargonidin at a dose of 1, 5 or 10 mg/kg in a mouse model of TNBS-induced colitis (Fig. 2). Clinical data and analysis of the macroscopic and microscopic

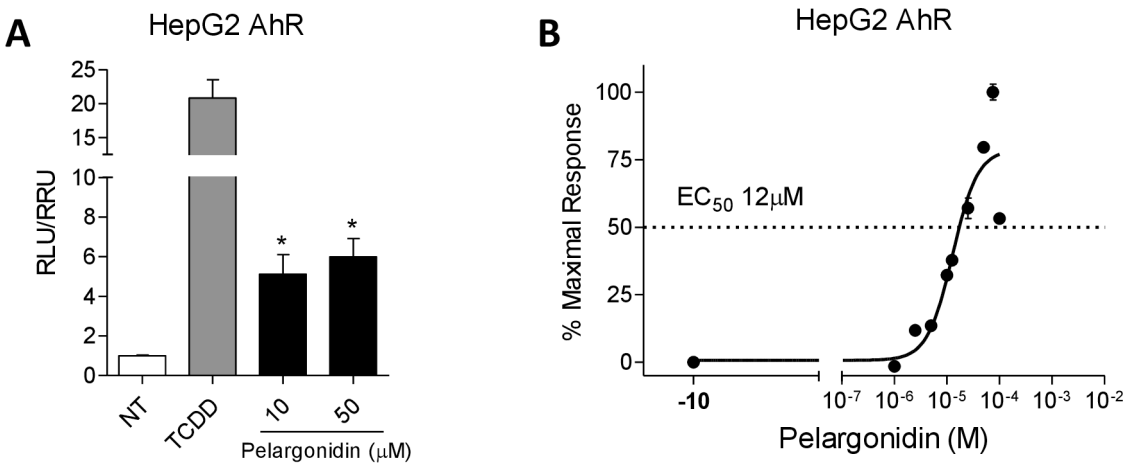

Fig. 1. Pelargonidin exerts its effects through the activation of the aryl hydrocarbon receptor (AHR). (A) Fold of induction of luciferase activity in cells transfected with *AHR* reporter gene and incubated with TCDD (5 nM) or Pelargonidin (10–50 μM). (B) Dose-response curve of pelargonidin to evaluate AHR activation; cells were stimulated with increasing concentrations of pelargonidin 1 μM to 100 μM. Results are expressed as mean ± standard error. * $p < 0.05$ versus not treated cells (NT).

features of the colon showed for doses of 1 and 5 mg/kg of pelargonidin a dose-dependent effect with the lowest dose exerting only mild beneficial effects. However, the 10 mg/kg dose, contrary to expectations, showed intermediate effects between the 1 and 5 mg/kg dose. Because these data suggest that 5 mg/kg of Pelargonidin was fully effective in reversing signs of intestinal inflammation we used this dose to further investigate the mechanism of action of pelargonidin on intestinal immunity. For this purpose, we induced a colon inflammation by administering TNBS to *Ahr*$^{+/+}$ and *Ahr*$^{-/-}$ mice. As shown previously by us and others, *Ahr*$^{-/-}$ mice are very susceptible to the TNBS colitis with high mortality rate [26]. In our experimental set we found a mortality rate of 80% in the *Ahr* knock-out group and therefore it was not possible to further investigate in this strain (data not shown). In wild-type mice, however, the severity of wasting disease and intestinal inflammation induced by TNBS was reversed by treatment with pelargonidin as measured by lower body weight lost, lower CDAI and by assessing the macroscopic and microscopic feature of the colon (Fig. 3A–D). We analyzed the colon expression of Ace2 protein and mRNA (Fig. 3E, F). Immunohistochemistry and qPCR confirmed that induction of colitis by administration of TNBS increased the expression of Ace2 both mRNA and protein as found in patients with IBD. In contrast, the administration of pelargonidin was able to counteract the increase in *Ace2* expression (Fig. 3E, F) [12]. To further confirm that pelargonidin administration in vivo activates the AHR receptor, we have evaluated the expression of one of the main AHR target genes, *Cyp1a1*. The data showed that pelargonidin administration up-regulates *Cyp1a1* expression in the colon (Fig. 3G). We then analyzed the colon expression of *Mas* and cytokines (Fig. 3F–J).

In this mouse model of colitis, we found exposure to TNBS promoted a strong upregulation of pro-inflammatory cytokines (Fig. 3I-J); *Il-1β* was up-regulated ≈20 times in the colon of TNBS-treated mice compared to naïve mice (Fig. 3I). Furthermore, a five fold increase in *Tnf-α* mRNA (Fig. 3J) was detected in mice exposed to TNBS. In contrast, *Mas* mRNA expression was decreased (Fig. 3H). Administering TNBS mice with pelargonidin reversed this pattern while induced the expression of *Tgf-β* (Fig. 3I–K). The anti-inflammatory effect exerted by pelargonidin also resulted in a strong reduction of *Ace2 mRNA* expression (Fig. 3F). The correlation analysis between *Il and 1β/Ace2* and *Tnf-α/Ace2* confirmed a statistically significant correlation between the expression of the two pro-inflammatory cytokines and *Ace2* (*Il-1β/Ace2 P value = 0.0244; Tnf-α/Ace2 P value < 0.0001)* (Fig. 3L, M). Again, there was a closer correlation between the expression of *Ace2* and that of *Tnf-α* (*Il-1β/Ace2 R squared = 0.1867; Tnf-α/Ace2 R squared = 0.7695)* (Fig. 3L, M).

Due to the inability to analyze the effects of pelargonidin treatment in the colitis model in *Ahr*$^{-/-}$ mice for the high mortality, to investigate whether the immunomodulatory effect exerted by Pelargonidin was mediated by binding on AHR, we tested the compound on murine macrophages purified from the spleen of *Ahr*$^{+/+}$ and *Ahr*$^{-/-}$ mice. Macrophages were subjected to pro-inflammatory stimuli (LPS + IFN-γ) and treated with pelargonidin for 16 h. Stimulation with LPS + IFN-γ induced an increase in the production of pro-inflammatory cytokines (Fig. 4A, B) and a reduction in the production of *Tgf-β* (Fig. 4C) in macrophages deriving from both genotypes. *Il-6* up-regulation was much higher in *Ahr*$^{-/-}$ macrophages compared to wild-type (Fig. 4E). Treatment with Pelargonidin reverted the pro-inflammatory polarization but only in wild-type macrophages, while it had no effect on *Ahr*$^{-/-}$ macrophages, underlining the role of the AHR receptor in the mechanism of action of Pelargonidin.

3.3. *Pelargonidin protects against colon inflammation induced by HFD-F and down-regulates Ace2 expression*

Taking into consideration obesity pandemia and that exposure to high caloric intake promotes a state of intestinal sub-inflammation, and that obesity is a well-defined risk factor for development of severe COVID19, we have tested the effects of Pelargonidin also in a mouse model of a high-fat/high-sugar diet [39–41].

In this model, *Ahr*$^{+/+}$ and *Ahr*$^{-/-}$ mice were treated with exposed a chronic high caloric [26] intake by feeding them a diet enriched cholesterol and fructose (HFD-F) for 8 weeks. Starting from the second week (day 8) an experimental group of mice for each genotype was treated with pelargonidin daily. As shown in Fig. 5, mice exposed to chronic high caloric intake gained significantly more body weight than mice feed a normal chow diet, and they had significantly higher BMI at the end of the study without significant differences between the two genotypes (Fig. 5A–C). Treating mice with 5 mg/kg/day Pelargonidin for 7 weeks protected against body weight gain and resulted in a lower BMI in comparison to mice feed an HFD-F alone (Fig. 5A–C). Instead, the beneficial effects exerted by Pelargonidin were completely abrogated in *Ahr*$^{-/-}$ mice (Fig. 5A–C). We have therefore focused our attention on intestinal inflammation. The histological analysis of the colon showed no major morphological abnormalities, although further functional assessment revealed a robust increase of intestinal permeability in the mice exposed to HFD-F (Fig. 5D, E). Treating mice with pelargonidin restored the normal colon permeability in wild-type mice, but had no beneficial effects in *Ahr*$^{-/-}$ mice which exhibited much more severe changes in permeability than in *Ahr*$^{+/+}$ mice (Fig. 5D, E).

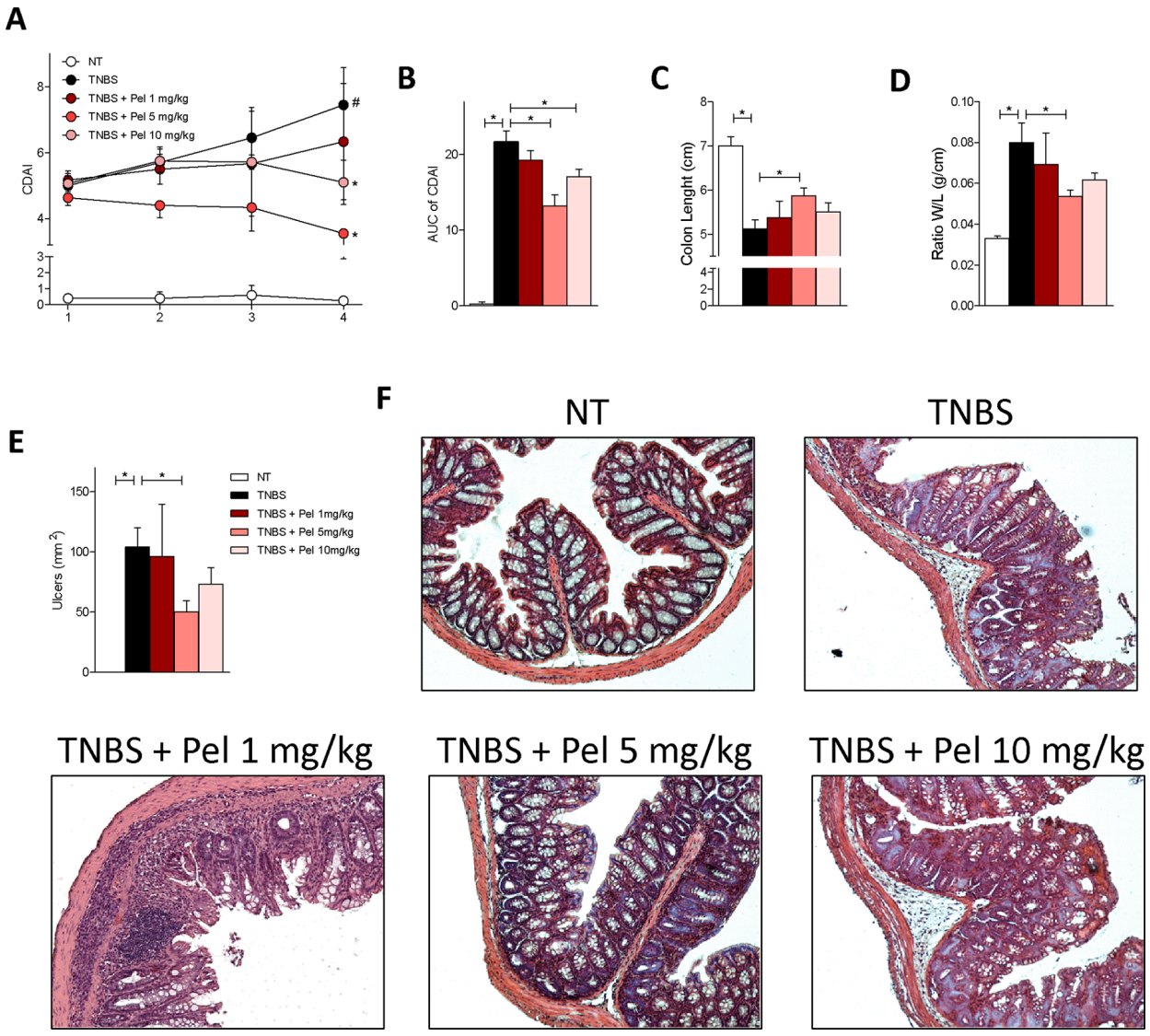

Fig. 2. Pelargonidin reduces the severity of TNBS colitis in a dose-dependent manner. Colitis was induced by TNBS. After induction of colitis the mice were treated daily with Pelargonidin (1, 5 or 10 mg/Kg) or vehicle. Disease was monitored by daily evaluation of (A) changes in colitis disease activity index (CDAI) and by evaluation of the (B) Area Under the Curve (AUC). At the end of the experiment, we evaluated (C) colon length (cm) and (D) ratio of colon weight/colon length (g/cm). (E) Area of ulcers and (F) H&E staining of colon sections (10× magnification) and Histological Score from each experimental group. Results are expressed as mean ± SEM (n = 5–7); In graph A # TNBS Vs NT; * TNBS + Pel Vs TNBS; in all graphs # and * $p < 0.05$.

Elevated colonic *ACE2* levels have been detected in the colon of IBD patients and are associated with inflammation and severe disease, suggesting a possible correlation between *ACE2* expression and colon inflammation in IBD patients [12]. We have therefore investigated the expression of *Ace2* and *Mas* in the colon and compared them with colon profiles of various cytokines (Fig. 5F–J). HFD-F increased *Ace2* expression and reduced *Mas* expression in both $Ahr^{+/+}$ and $Ahr^{-/-}$ mice, while increased the colon expression of *Il-1β* and *Tnf-α* and downregulated the *Tgf-β mRNA*. Pelargonidin treatment reversed the inflammatory pattern by down-regulating the expression of both *Il-1β* and *Tnf-α,* but only in $Ahr^{+/+}$ mice. In wild-type mice exposure to the anthocyanin also reduced the expression of *Ace2*, bringing it back to the value measured in untreated wild-type mice, while exerted only a slight effect on the expression of *Mas* mRNA (Fig. 2F–J). To investigate whether there was also in this mouse models with a mild inflammation in the colon, a direct correlation between the expression of *Ace2* and pro-inflammatory cytokines, we performed correlation analyses between *Il and 1β* and *Ace2* and between *Tnf-α* and *Ace2.* As shown in Fig. 5K and L, the colon levels of the two cytokines were positively correlated with *Ace2* expression in both $Ahr^{+/+}$ and $Ahr^{-/-}$ mice. The fact that the R squared value was greater in the *Tnf-α/Ace2* correlation than *Il-1β*/Ace2 confirmed a stronger correlation between the expression of *Ace2* and *Tnf-α*.

3.4. *In vitro characterization of pelargonidin effects on intestinal epithelial cells*

Because, *ACE2* expression in the intestine is highly restricted to epithelial cells, we have then examined whether exposure of Caco-2 cells, a human intestinal epithelial cell line, to TNF-α modulates the expression of *ACE2*. The results of these experiments demonstrated that exposure to TNF-α promotes the expression of pro-inflammatory genes *IL-8*, *IL-6* and *IL-1B* by Caco-2 cells (Fig. 6B–D) and increased the expression of *Ace2* (≈2.5 times) confirming the close correlation between TNF-α and *ACE2* (Fig. 6A). Administration of Pelargonidin reversed this pattern in a concentration-dependent manner (Fig. 6A–D).

To investigate the molecular mechanism behind the correlation between TNF-α and *ACE2* and behind the beneficial effect exerted by Pelargonidin, we purified intestinal epithelial cells (IECs) from the colon

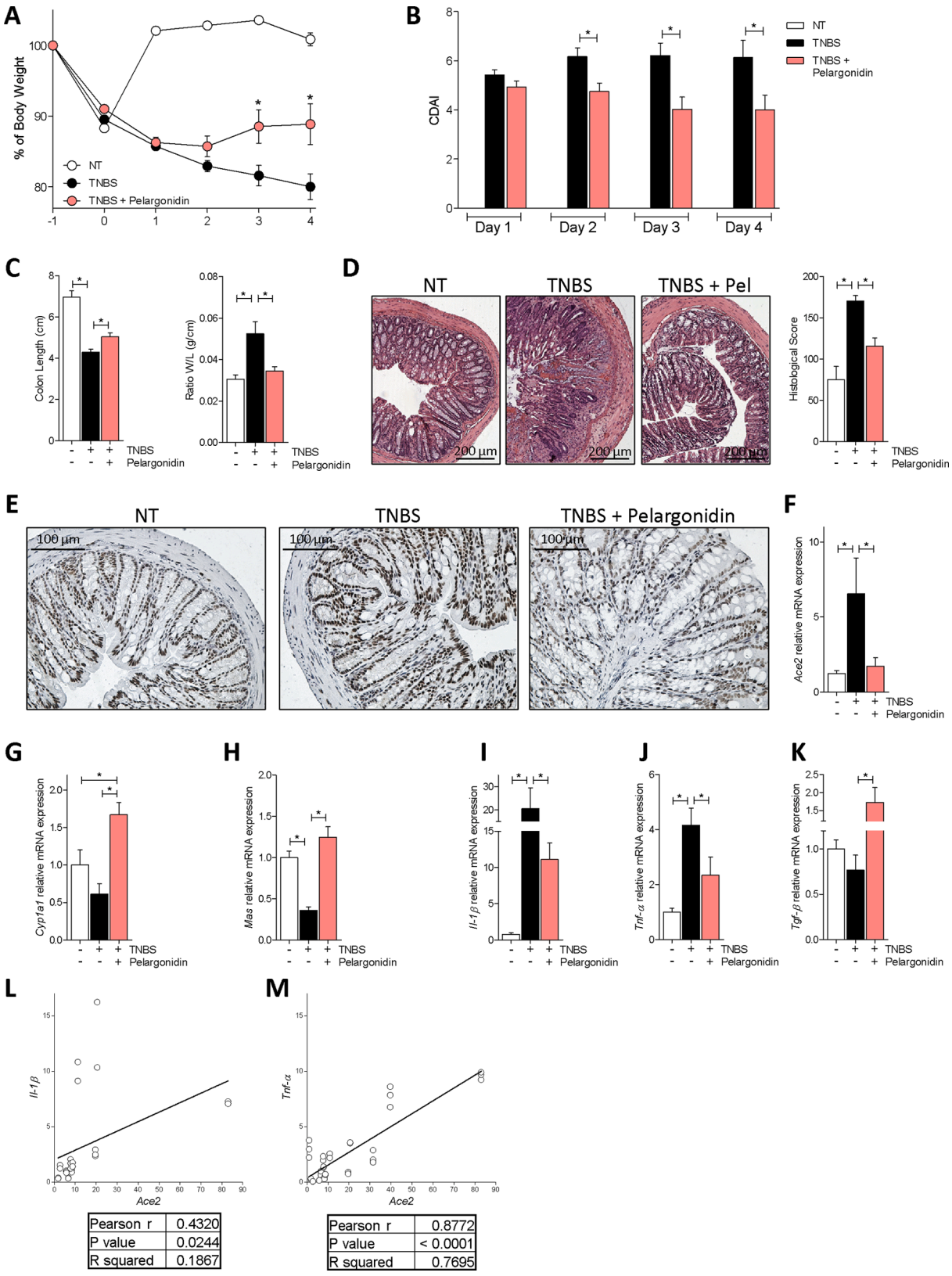

Fig. 3. Pelargonidin effect on acute colitis. Colitis was induced by TNBS. After induction of colitis the mice were treated daily with Pelargonidin (5 mg/Kg) or vehicle. Disease was monitored by daily evaluation of (A) changes in body weight (%), (B) colitis disease activity index (CDAI), (C) colon length (cm) and ratio of colon weight/colon length (g/cm). (D) H&E staining of colon sections (10× magnification) and Histological Score from each experimental group. (E) The figure shows immunohistochemistry representative images of the colon of one mouse for each experimental group stained with anti-ACE2 Ab (20x magnification). RNA extracted from colon was used to evaluate, by quantitative real-time PCR, the relative mRNA expression of (F) *Ace2,* (G) *Cyp1a1*, (H) *Mas*, (I) *Il-1β*, (J) *Tnf-α* and (K) *Tgf-β*. Values are normalized relative to *Gapdh* mRNA. The values are expressed relative to those of control group (NT) which are arbitrarily set to one. Correlation

graph of *Ace2* mRNA expression and (L) *Il-1β* (M) *Tnf-α*. Results are expressed as mean ± SEM (n = 7–12); In graph A * TNBS + Pelargonidin Vs TNBS; in all graphs * $p < 0.05$.

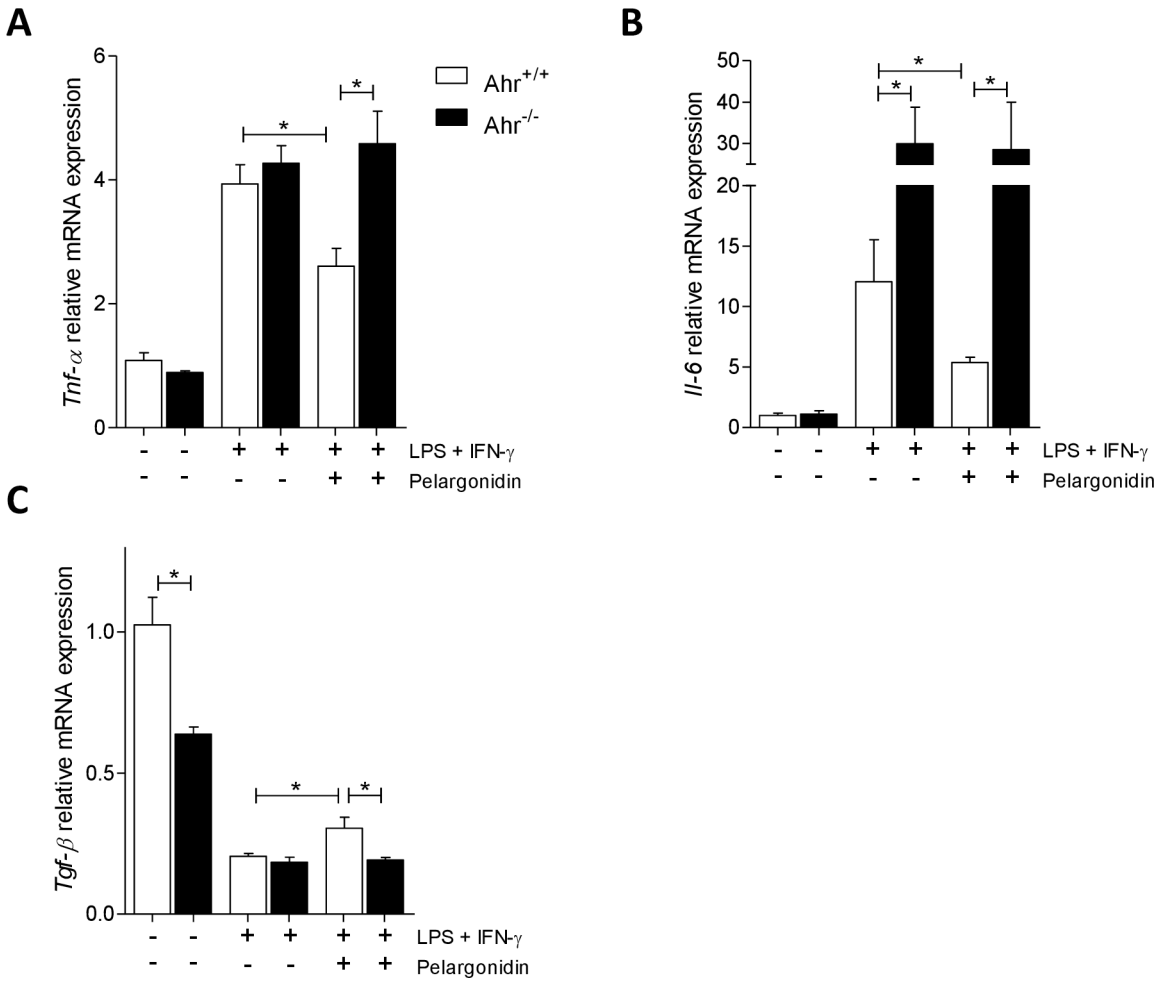

Fig. 4. Pelargonidin exert immunomodulatory effects through AHR. Spleen macrophages purified from $AhR^{+/+}$ and $AhR^{-/-}$ mice were activated *in vitro* with LPS (5 ng/mL) in combination with IFN-γ (20 ng/mL) alone or plus Pelergonidin (20 μM) for 16 h. At the end of stimulation, the relative mRNA expression of pro-inflammatory cytokines (C) *Tnf-α* and (D) *Il-6*, and anti-inflammatory cytokines (E) *Tgf-β*, was evaluated by Real-Time PCR. Values are normalized relative to Gapdh mRNA and the values are expressed relative to those of control group which are arbitrarily set to one. Results are the mean ± SEM (n = 6); * $p < 0.05$.

of $Ahr^{+/+}$ and $Ahr^{-/-}$ mice and stimulated them with TNF-α. By analyzing the expression of the *Ace2* and *Il-6* genes we demonstrated that also in these primary murine intestinal epithelial cells TNF-α induces inflammation by up-regulating both genes (Fig. 7A and B). Furthermore, the absence of the AHR receptor exacerbated the inflammation induced by TNF-α. Pelargonidin reverted the upregulation of both genes in a concentration-dependent manner but only in cells purified from wild-type mice (Fig. 7A and B). In $Ahr^{-/-}$ mice, the absence of the receptor abrogated the beneficial effect exerted by Pelargonidin. It is known that TNF-α, through its receptor, induces the transcription of several pro-inflammatory genes by activating the NF-kB pathway [42,43]. For this reason, we have investigated the effect of NF-kB pathway inhibition on Ace2 expression. Administration of an NF-κB inhibitor was able to down-regulate the expression of *Ace2* and *Il-6* in both wild-type and knock-out cells confirming that the mechanism by which TNF-α up-regulate *Ace2* and *Il-6* involves the activation of NF-κB.

Since ACE2 represents the host receptor used by the SARS-Cov2 virus to invade cells, and reducing the expression of *ACE2* might represent an interesting host defense mechanism against virus invasion. In this context we also investigated whether Pelargonidin was able to reduce the binding of the viral Spike protein on ACE2 (Fig. 8).

We therefore investigated, through docking calculations, the possibility of Pelargonidin to bind several pockets suggested in previous studies: i) the hydrophobic pockets on the b-sheet core of the RBD [44], ii) the fatty acid (FA) pocket identified by Toelzer *et al.* [33,45]. and finally, iii) the flavonoids binding pocket suggested by Allam *et al.* [46]. All docking calculations were performed using Glide software package. The scores of the best poses highlighted a marked preference of the results obtained in the FA pocket (best docking score −7.7 kcal/mol), with respect to the results obtained in the hydrophobic pockets on the b-sheet core of the RBD (best docking score −5.2 kcal/mol) or in the pocket proposed by Allam (best docking score −5.8 kcal/mol), thus suggesting that Pelargonidin binds the FA pocket on the RBD of Spike, as already reported for other highly unsaturated naturally occurring compounds (e.g. Vitamin k, retinoids) [45]. Analysis of the best scored and clustered docking pose in the FA pocket (Fig. 8A–C) showed the Pelargonidin polyphenolic ring contacting with Leu368, Leu387, Phe388, Phe342 and Ile434. Furthermore, Phe377 makes a p-cation interaction with the oxygen of the ring C, whereas Tyr365 and Tyr369 are engaged in a p-p stacking with the biphenyl ring and with the ring B, respectively. Finally, the binding mode is further stabilized by the H-bond formed between the ring B hydroxyl group and the backbone of Ala372.

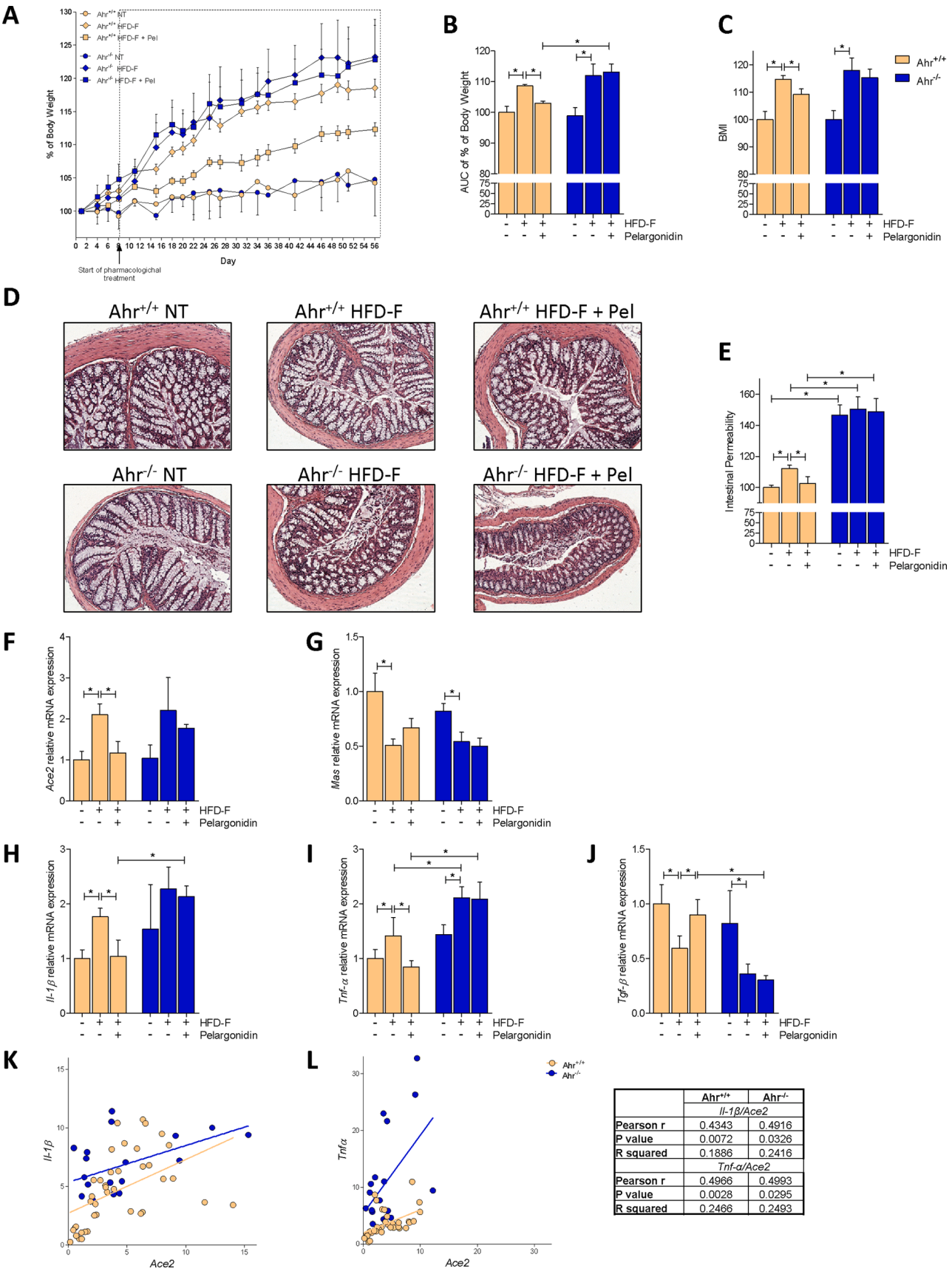

	Ahr+/+	Ahr-/-
	Il-1β/Ace2	
Pearson r	0.4343	0.4916
P value	0.0072	0.0326
R squared	0.1886	0.2416
	Tnf-α/Ace2	
Pearson r	0.4966	0.4993
P value	0.0028	0.0295
R squared	0.2466	0.2493

(caption on next page)

Fig. 5. Benefit of Pelargonidin administration in mouse model of NASH is lost in *Ahr*$^{-/-}$ strains. C57BL/6 male mice, (*Ahr*$^{+/+}$) and their congenic littermates *Ahr* knock out (*Ahr*$^{-/-}$) were fed a normal chow diet (NT) or a high fat diet with fructose in water (HFD-F) as described in Material and Methods section. (A) Changes in body weight (%) assessed for 56 days. (B) Areas under curve (AUC) of body weight expressed in arbitrary units. (C) Body Mass Index (BMI) is calculated at the end of the study as the ratio between body weight (g) and body length^2 (cm^2). (D) Histological sections, performed with H&E staining on colon (10x magnification) of *Ahr*$^{+/+}$ and *Ahr* $^{-/-}$ mice for each experimental group. (E) Intestinal permeability was measured after 4 weeks of diet with FITC-dextran administration. At the end of experiment the total RNA extracted from colon was used to evaluate, by quantitative real-time PCR, the relative mRNA expression of (F) *Ace2*, (G) *Mas*, (H) *Il-1β*, (I) *Tnf-α*, (J) *Tgf-β*. Values are normalized relative to *Gapdh* mRNA. The values are expressed relative to those of control group (NT) which are arbitrarily set to one. Correlation graph of Ace2 mRNA expression and (K) *Il-1β* (L) *Tnf-α*. Results are expressed as mean ± SEM (n = 6–10); * $p < 0.05$.

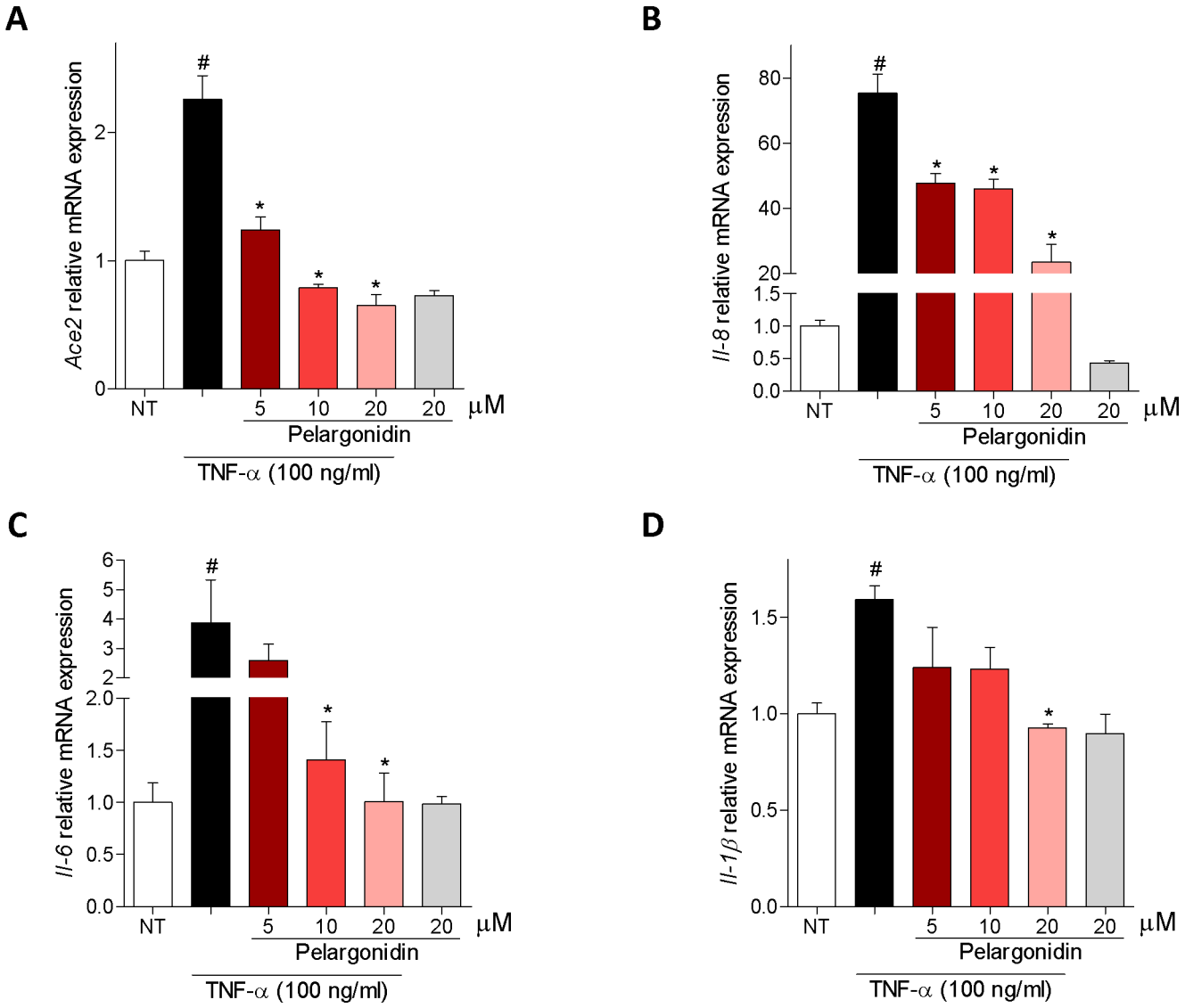

Fig. 6. Pelargonidin counteract TNF-α-inflammatory activation on Caco2-cells. Caco-2 cells, a human intestinal epithelial cell line, activated with TNF-α 100 ng/ml for 24 h alone or in combination with pelargonidin (5, 10, and 20 μM). At the end of stimulation, the relative mRNA expression of (A) *ACE2*, (B) *IL-8*, (C) *IL-6* and (D) *IL-1B*, was evaluated by Real-Time PCR. Values are normalized relative to Gapdh mRNA and the values are expressed relative to those of control group (NT) which are arbitrarily set to one. Results are the mean ± SEM (n = 5); # NT Vs TNF-α; * TNF-α Vs TNF-α + Pelargonidin; # and * $p < 0.05$.

Given the results of the docking calculations, we have then investigated whether the Pelargonidin impact on the binding of S protein to the ACE2 receptor. For this purpose, a Spike/ACE2 Inhibitor Screening Assay Kit was used.

The results obtained by us showed that pelargonidin was able to reduce binding in a concentration-dependent manner. At the highest tested concentration, equal to 50 μM, we measured a reduction in Spike binding on ACE2 of about 40% (Fig. 8D). To confirm this data, we also performed a SARS-CoV-2 virus infection test on Vero E6 cell line, kidney epithelial cells extracted from monkey. In this assay, pelargonidin showed an ability to reduce virus entry, measured by plaque assay, of approximately 70% at the highest concentration of 100 μM (Fig. 8E).

The data obtained from docking and *in vitro* tests associated with the down-regulation of *ACE2* expression exerted by Pelargonidin and the anti-inflammatory activity make pelargonidin very interesting in the prevention and treatment of SARS-Cov-2 infection.

4. Discussion

ACE2, the SARS CoV2 receptor, in widely expressed in the

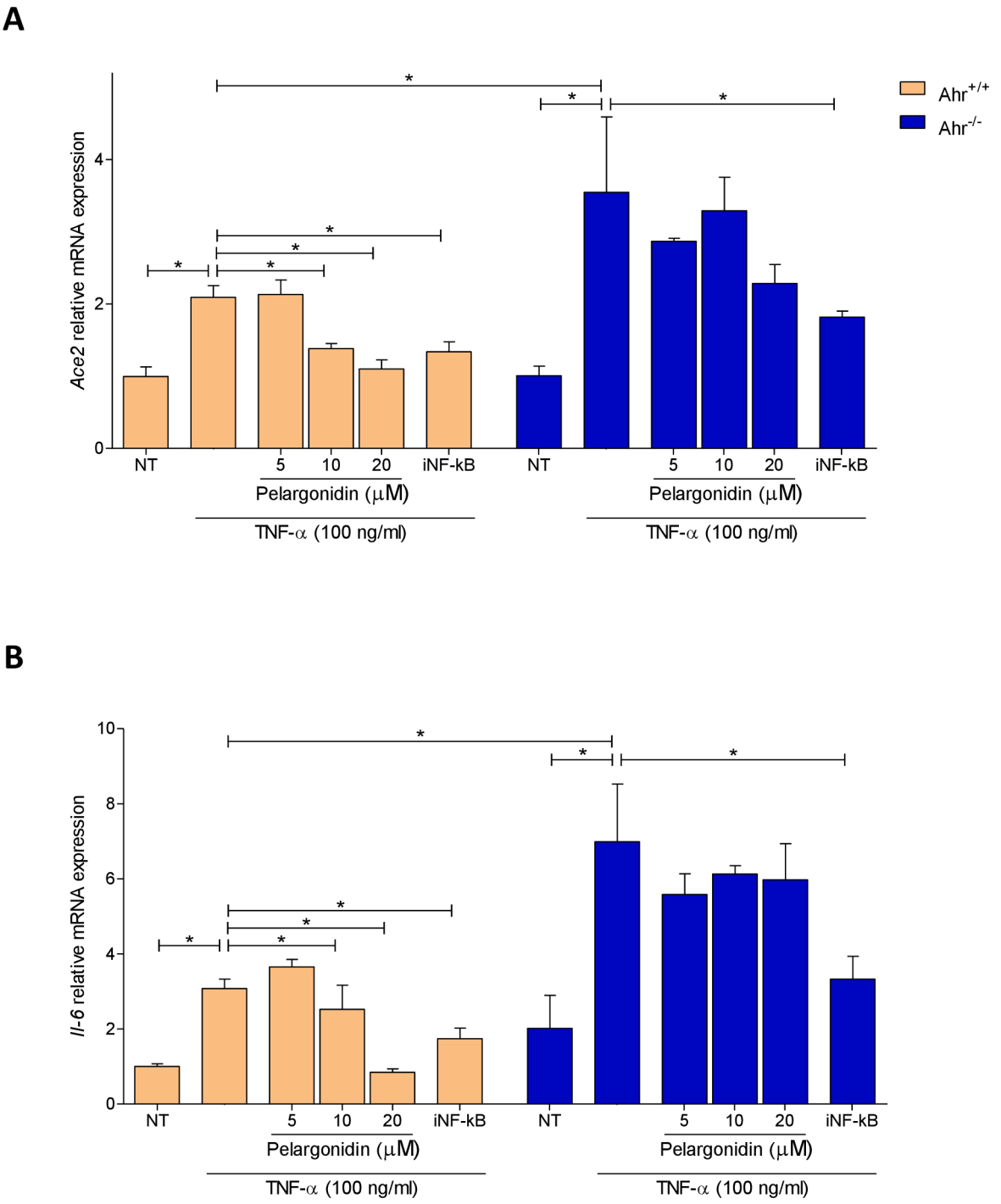

Fig. 7. TNF-α up-regulates *Ace2* expression by NF-kB on intestinal epithelial cells and pelargonidin inhibits this pathway by activating AHR. Intestinal epithelial cells were purified from the colon of $Ahr^{+/+}$ and $Ahr^{-/-}$ mice. Intestinal epithelial cells were cultured for 24 h with TNF-α 100 ng/ml and treated with Pelargonidin (5, 10, and 20 μM) or with the NF-κB inhibitor (iNF-kB 100 nM). At the end of stimulation, the relative mRNA expression of (A) *Ace2* and (B) *Il-6* was evaluated by Real-Time PCR. Values are normalized relative to *Gapdh* mRNA and the values are expressed relative to those of control group ($Ahr^{+/+}$ NT) which are arbitrarily set to one. are expressed as mean ± SEM (n = 5); * $p < 0.05$.

gastrointestinal tract, although the terminal ileum is one of the human body tissues with the highest expression of the receptor [21]. In the ileum, ACE2 regulates amino acids uptake and is essential for nutrients absorption. The receptor is also expressed in normal human colon, thought at significantly lower levels than the ileum, but its functional role in this portion of the intestine is less defined. Of relevance, however, the expression of *ACE2* in the two tissues undergoes an opposite regulation in response to inflammation. Thus, while the ileal expression of *ACE2* is reduced in patients with active Crohn's disease of the ileum, the colonic expression of the receptor is robustly induced in patients with ulcerative colitis or Crohn's disease showing a colon involvement [47]. Further on, a linear correlation has been detected linking the severity of colon inflammation, colon expression of expression of pro-inflammatory cytokines including *IFN-γ, TNF-α, IL-1β,* and *IL-6* and the expression of *ACE2 mRNA* [12,13,48,49]. This inflammation-modulated expression of *Ace2* in the colon show similarity with the receptor regulation in the

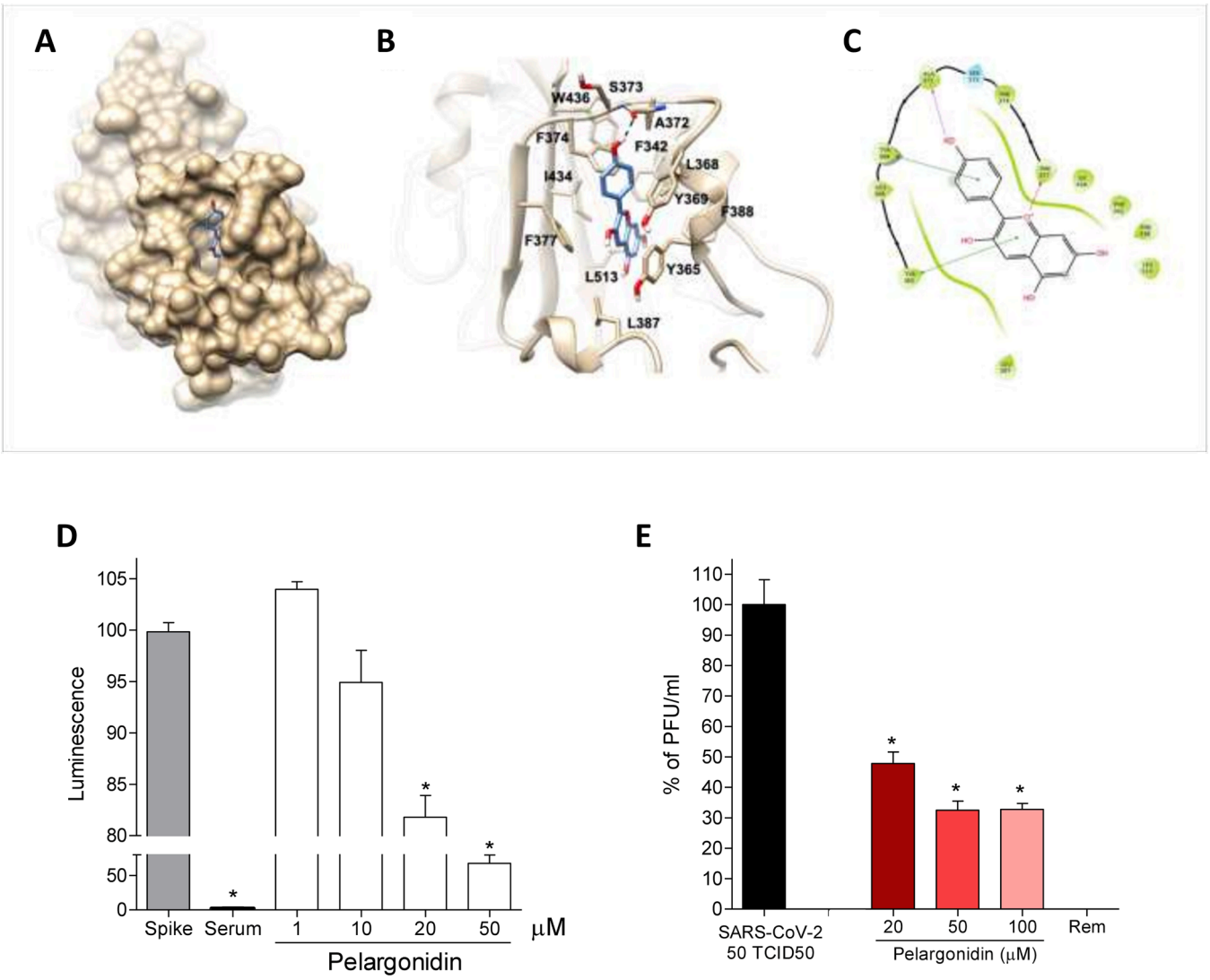

Fig. 8. Pelargonidin inhibits binding of the SARS-Cov-2 virus on the host cells. (A) Hydrophobic FA binding pocket in a surface representation; (B) Cartoon representation of binding mode of pelargonidin to SARS-CoV-2 receptor. The ligand is represented as blue sticks, whereas the interacting residues of the receptor are shown in tan and labelled. Oxygen atoms are depicted in red and nitrogens in blue. The receptors are represented as tan ribbons. Hydrogens are omitted for the sake of clarity; (C) Diagram of Pelargonidin interaction. (D) SARS-CoV-2 Spike binding to immobilized ACE2; Luminescence was measured using a Fluo-Star Omega fluorescent microplate reader. Pelargonidin was tested at different concentration (1, 10, 20 and 50 μM), to evaluate their ability to inhibit the binding of Spike protein (5 nM) to immobilized ACE2, by using the ACE2:SARS-CoV-2 Spike Inhibitor Screening assay Kit. Results are expressed as mean ± SEM (n = 5); * $p < 0.05$. To confirm the validity of the assay used in this study, we tested plasma samples of post COVID-19 patients as a control. (E) Virus growth in Vero 6E cells analyzed by plaque assay. Pelargonidin was tested at concentration of 20, 50 and 100 μM. To confirm the validity of the assay used in this study, we tested Remdesivir.

lung, the target tissue of COVID19 [10,50]. It is now well established that *the* expression of the receptor in alveolar cells increases in a cytokine dependent manner in response to SARS-CoV2 infection, with a direct correlation with the tissue expression of IFN-γ. While these data highlight a potential role for an inflammatory network in promoting intestinal ACE2 expression, the molecular mechanisms involved in its conter-regulation remains elusive. To answer this question, we have settled up a study to investigate the role of the AHR in regulating *Ace2* expression in mouse models of IBD. Additionally, since obesity and diabetes promote a state of sub-inflammation in the gastrointestinal tract [51,52] and it are two well-defined risk factors for developing severe COVID19, we have investigated whether this regulation is maintained in mice exposed to a high caloric intake.

Gastrointestinal symptoms, including vomiting, diarrhea, or abdominal pain of various severity, occurs frequently in the early stage of COVID19, highlighting the role of intestinal ACCE in promoting SARS CoV2 infection. This view is of specific relevance in patients with IBD. Two recent studies [53,54] have shown that SARS CoV2 virus might directly infect the human gut, and therefore the modulation of *ACE2* expression in the gastrointestinal tract might have therapeutic relevance in reducing the virus load. The data we have gathered from the two mouse models of IBD strongly support the notion that upregulation of *Ace2* in the colon is due to a state of inflammation marked by strong induction of pro-inflammatory cytokines [47,55]. Importantly, in contrast to *Ace2* the expression of the Ang 1–7 receptor *Mas*, was markedly downregulated in both models (Figs. 3 and 5). The correlation

of Ace2 mRNA expression with the levels of inflammatory biomarkers was very stringent. Indeed, while in the TNBS model the levels of various cytokines were increased by 5–20 folds and the expression of *Ace2* mRNA was induced by ≈7-fold in comparison to naive mice (Fig. 3E), in the HFD-F model only a mild inflammation was detected and the levels of *Il-1β* and *Tnf-α* and Ace2 mRNA levels were increased by approximately two-folds (Fig. 5H–J). Moreover, in the colon of animals subjected to a high-calorie intake, the expression of *Mas* was halved in comparison to that in mice fed a chow-diet (Fig. 5F, G). These data establish, across the various models, a direct correlation between the severity of colon inflammation and *Ace2* gene transcription.

In both mouse models we have found that values of R squared indicated a close correlation between the expression of *Ace2* and *Tnf-α*. These data are deeply consistent with the finding that in IBD patients, anti-*TNF-α* therapies negatively regulate ACE2 expression in the colon [12,56]. Confirmation of the direct regulation of *ACE2* expression by *TNF-α* was given obtained also by results of *in vitro* experiment, since exposure of human intestinal epithelial cells, Caco 2, to TNF-α directly up-regulates the expression of *ACE2* (Fig. 6A).

Similarly, to other flavonoids, pelargonidin, a common constituent of many red plant foods, including berries, grapes or cabbage, have been used in the traditional medicine in the treatment of a number of human alignments [57,58]. Pelargonidin display a several biological activities, the most prominent being those related to their anti-oxidant effects. We have confirmed in this study that pelargonidin exerts anti-inflammatory effects in intestine in mouse models of IBD and obesity through the interaction with the AHR. Treatment with pelargonidin reduced the expression of pro-inflammatory cytokines in the colon in both models of intestinal inflammation, alleviating the disease (Figs. 2, 3 and 5). Furthermore, treatment with Pelargonidin restored *Ace2* expression to the level measured in the colon of naive mice (Figs. 3E and 5F). The beneficial effects exerted by the compound were abrogated in the absence of *AhR* confirming the functional relevance of the receptor in mediating the anti-inflammatory activities of this flavonoid (Figs. 4, 5 and 7). *In vitro* studies also confirmed that pelargonidin might directly inhibit *ACE2* induction caused by exposure of human intestinal epithelial cell line to the TNF- α (Fig. 6). Moreover, through the use of an NF-κB inhibitor, we have shown that the up-regulation of *ACE2* by TNF-α is mediated by the activation of NF-κB (Fig. 7). Using intestinal epithelial cells purified from wild-type and $Ahr^{-/-}$ mice we showed that the effect of down-regulating of *Ace2* exerted by Pelargonidin requires the presence of AHR (Fig. 7). As demonstrated in other studies, the activated AHR receptor can exert anti-inflammatory effects by inhibiting the NF-kB pathway [59,60].

The regulatory effects of pelargonidin on the intestinal *ACE2* expression might be of relevance in the context of SARS-CoV-2 infection, since high levels of ACE2 are compatible with an increased risk of SARS-CoV-2 uptake by the inflamed colon [12]. Importantly, in addition to *ACE2* regulation, we have shown that beneficial effects of Pelargonidin might extend to a direct regulation of SARS-CoV-2/ACE2 interaction. Indeed, we found that Pelargonidin not only reduces the interaction between ACE2 and the Spike protein of the SARS-Cov-2 but also reduces the ability of the SARS-CoV-2 to infect Vero E6 cell line, a monkey kidney epithelial cell line used to investigate the SARs-CoV-2 replication (Fig. 8). We have investigated the molecular mechanisms involved in preventing the binding of SARS-CoV2 virus to its receptor identifying the fatty acid binding pocket in the RBD as the putative binding site of pelargonidin.

In summary we shown that the natural flavonoid, Pelargonidin, reverses *Ace2* induction in rodent models of inflammation and this effect is mediated by AHR. In addition, the Pelargonidin might reduce SARS-CoV-2/ACE2 interaction affecting the virus uptake and replication. These data highlight the potential of natural agents in reducing inflammation and invasion by SARS-CoV-2.

CRediT authorship contribution statement

Michele Biagioli: Conceptualization, Investigation, Data curation, Writing - original draft. **Silvia Marchianò:** Investigation, Data curation. **Rosalinda Roselli:** Investigation, Data curation. **Cristina Di Giorgio:** Investigation, Data curation. **Rachele Bellini:** Investigation, Data curation. **Martina Bordoni:** Investigation, Data curation. **Anna Gidari:** Methodology, Data curation. **Samuele Sabbatini:** Methodology, Data curation. **Daniela Francisci:** Conceptualization, Supervision. **Bianca Fiorillo:** Investigation, Data curation. **Bruno Catalanotti:** Conceptualization, Writing - review & editing. **Eleonora Distrutti:** Conceptualization, Writing - review & editing. **Adriana Carino:** Investigation, Data curation. **Angela Zampella:** Conceptualization, Writing - review & editing, Funding acquisition. **Gabriele Costantino:** Conceptualization, Resources, Writing - review & editing. **Stefano Fiorucci:** Conceptualization, Writing - original draft, Funding acquisition.

Declaration of Competing Interest

The authors declare that they have no known competing financial interests or personal relationships that could have appeared to influence the work reported in this paper.

Acknowledgments

We thank the Italian MIUR/PRIN 2017 (2017FJZZRC) for partially supporting the research activity. The authors thank to Sabrina Bastianelli, Sara Pierucci and Chiara Busti for their technical contributions to the project.

References

[1] N. Zhu, D. Zhang, W. Wang, X. Li, B. Yang, J. Song, X. Zhao, B. Huang, W. Shi, R. Lu, P. Niu, F. Zhan, X. Ma, D. Wang, W. Xu, G. Wu, G.F. Gao, W. Tan, A novel coronavirus from patients with pneumonia in China, 2019, N. Engl. J. Med. 382 (8) (2020) 727–733.

[2] R. Yan, Y. Zhang, Y. Li, L. Xia, Y. Guo, Q. Zhou, Structural basis for the recognition of SARS-CoV-2 by full-length human ACE2, Science 367 (6485) (2020) 1444–1448.

[3] M. Gui, W. Song, H. Zhou, J. Xu, S. Chen, Y. Xiang, X. Wang, Cryo-electron microscopy structures of the SARS-CoV spike glycoprotein reveal a prerequisite conformational state for receptor binding, Cell Res. 27 (1) (2017) 119–129.

[4] Q. Wang, Y. Zhang, L. Wu, S. Niu, C. Song, Z. Zhang, G. Lu, C. Qiao, Y. Hu, K. Y. Yuen, H. Zhou, J. Yan, J. Qi, Structural and Functional Basis of SARS-CoV-2 Entry by Using Human ACE2, Cell 181 (4) (2020) 894–904.e9.

[5] Y. Yuan, D. Cao, Y. Zhang, J. Ma, J. Qi, Q. Wang, G. Lu, Y. Wu, J. Yan, Y. Shi, X. Zhang, G.F. Gao, Cryo-EM structures of MERS-CoV and SARS-CoV spike glycoproteins reveal the dynamic receptor binding domains, Nat. Commun. 8 (2017) 15092.

[6] A.C. Walls, X. Xiong, Y.J. Park, M.A. Tortorici, J. Snijder, J. Quispe, E. Cameroni, R. Gopal, M. Dai, A. Lanzavecchia, M. Zambon, F.A. Rey, D. Corti, D. Veesler, Unexpected receptor functional mimicry elucidates activation of coronavirus fusion, Cell 183 (6) (2020) 1732.

[7] A.C. Walls, Y.J. Park, M.A. Tortorici, A. Wall, A.T. McGuire, D. Veesler, Structure, function, and antigenicity of the SARS-CoV-2 Spike Glycoprotein, Cell 181 (2) (2020) 281–292.e6.

[8] G. Li, X. He, L. Zhang, Q. Ran, J. Wang, A. Xiong, D. Wu, F. Chen, J. Sun, C. Chang, Assessing ACE2 expression patterns in lung tissues in the pathogenesis of COVID-19, J. Autoimmun. 112 (2020), 102463.

[9] A.A. Valyaeva, A.A. Zharikova, A.S. Kasianov, Y.S. Vassetzky, E.V. Sheval, Expression of SARS-CoV-2 entry factors in lung epithelial stem cells and its potential implications for COVID-19, Sci. Rep. 10 (1) (2020) 17772.

[10] C.G.K. Ziegler, S.J. Allon, S.K. Nyquist, I.M. Mbano, V.N. Miao, C.N. Tzouanas, Y. Cao, A.S. Yousif, J. Bals, B.M. Hauser, J. Feldman, C. Muus, M. H. Wadsworth 2nd, S.W. Kazer, T.K. Hughes, B. Doran, G.J. Gatter, M. Vukovic, F. Taliaferro, B.E. Mead, Z. Guo, J.P. Wang, D. Gras, M. Plaisant, M. Ansari, I. Angelidis, H. Adler, J.M.S. Sucre, C.J. Taylor, B. Lin, A. Waghray, V. Mitsialis, D. F. Dwyer, K.M. Buchheit, J.A. Boyce, N.A. Barrett, T.M. Laidlaw, S.L. Carroll, L. Colonna, V. Tkachev, C.W. Peterson, A. Yu, H.B. Zheng, H.P. Gideon, C. G. Winchell, P.L. Lin, C.D. Bingle, S.B. Snapper, J.A. Kropski, F.J. Theis, H. B. Schiller, L.E. Zaragosi, P. Barbry, A. Leslie, H.P. Kiem, J.L. Flynn, S.M. Fortune, B. Berger, R.W. Finberg, L.S. Kean, M. Garber, A.G. Schmidt, D. Lingwood, A. K. Shalek, J. Ordovas-Montanes, SARS-CoV-2 Receptor ACE2 Is an Interferon-Stimulated gene in human airway epithelial cells and is detected in specific cell subsets across tissues, Cell 181 (5) (2020) 1016–1035.e19.

[11] J. Xu, M. Chu, F. Zhong, X. Tan, G. Tang, J. Mai, N. Lai, C. Guan, Y. Liang, G. Liao, Digestive symptoms of COVID-19 and expression of ACE2 in digestive tract organs, Cell Death Discov. 6 (2020) 76.

[12] A.A. Potdar, S. Dube, T. Naito, K. Li, G. Botwin, T. Haritunians, D. Li, D. Casero, S. Yang, J. Bilsborough, J.G. Perrigoue, L.A. Denson, M. Daly, S.R. Targan, P. Fleshner, J. Braun, S. Kugathasan, T.S. Stappenbeck, D.P.B. McGovern, Altered Intestinal ACE2 levels are associated with inflammation, severe disease, and response to anti-cytokine therapy in inflammatory bowel disease, Gastroenterology (2020).

[13] T. Toyonaga, K.C. Araba, M.M. Kennedy, B.P. Keith, E.A. Wolber, C. Beasley, E.C. Steinbach, M.R. Schaner, A. Jain, M.D. Long, E.L. Barnes, H.H. Herfarth, K.L. Isaacs, J.J. Hansen, M. Kapadia, J. Gaston Guillem, M.J. Koruda, R. Rahbar, T. Sadiq, A.S. Gulati, P. Sethupathy, T.S. Furey, C. Ehre, S.Z. Sheikh, Increased Colonic Expression of ACE2 Associates with Poor Prognosis in Crohn's disease, bioRxiv (2020).

[14] A.A. Potdar, S. Dube, T. Naito, G. Botwin, T. Haritunians, D. Li, S. Yang, J. Bilsborough, L.A. Denson, M. Daly, S.R. Targan, P. Fleshner, J. Braun, S. Kugathasan, T.S. Stappenbeck, D.P.B. McGovern, Reduced expression of COVID-19 host receptor, ACE2 is associated with small bowel inflammation, more severe disease, and response to anti-TNF therapy in Crohn's disease, medRxiv (2020).

[15] B. Verstockt, S. Verstockt, S. Abdu Rahiman, B.J. Ke, K. Arnauts, I. Cleynen, J. Sabino, M. Ferrante, G. Matteoli, S. Vermeire, Intestinal receptor of SARS-CoV-2 in inflamed IBD tissue seems downregulated by HNF4A in ileum and upregulated by interferon regulating factors in colon, J. Crohns Colitis (2020).

[16] P.D.R. Higgins, S. Ng, S. Danese, K. Rao, The Risk of SARS-CoV-2 in Immunosuppressed IBD Patients, Crohns Colitis 360 2 (2) (2020) otaa026.

[17] B. Lamas, J.M. Natividad, H. Sokol, Aryl hydrocarbon receptor and intestinal immunity, Mucosal Immunol. 11 (4) (2018) 1024–1038.

[18] M.S. Denison, A.A. Soshilov, G. He, D.E. DeGroot, B. Zhao, Exactly the same but different: promiscuity and diversity in the molecular mechanisms of action of the aryl hydrocarbon (dioxin) receptor, Toxicol. Sci. 124 (1) (2011) 1–22.

[19] L. Zhou, AHR function in lymphocytes: Emerging Concepts, Trends Immunol. 37 (1) (2016) 17–31.

[20] M. Garg, S.G. Royce, C. Tikellis, C. Shallue, D. Batu, E. Velkoska, L.M. Burrell, S. K. Patel, L. Beswick, A. Jackson, K. Britto, M. Lukies, P. Sluka, H. Wardan, Y. Hirokawa, C.W. Tan, M. Faux, A.W. Burgess, P. Hosking, S. Monagle, M. Thomas, P.R. Gibson, J. Lubel, Imbalance of the renin-angiotensin system may contribute to inflammation and fibrosis in IBD: A novel therapeutic target? Gut 69 (5) (2020) 841–851.

[21] T. Hashimoto, T. Perlot, A. Rehman, J. Trichereau, H. Ishiguro, M. Paolino, V. Sigl, T. Hanada, R. Hanada, S. Lipinski, B. Wild, S.M. Camargo, D. Singer, A. Richter, K. Kuba, A. Fukamizu, S. Schreiber, H. Clevers, F. Verrey, P. Rosenstiel, J. M. Penninger, ACE2 links amino acid malnutrition to microbial ecology and intestinal inflammation, Nature 487 (7408) (2012) 477–481.

[22] G. Mazza, Compositional and functional properties of saskatoon berry and blueberry, Int. J. Fruit Sci. 5 (3) (2005) 101–120.

[23] A. Jennings, A.A. Welch, S.J. Fairweather-Tait, C. Kay, A.M. Minihane, P. Chowienczyk, B. Jiang, M. Cecelja, T. Spector, A. Macgregor, A. Cassidy, Higher anthocyanin intake is associated with lower arterial stiffness and central blood pressure in women, Am. J. Clin. Nutr. 96 (4) (2012) 781–788.

[24] M. Pervin, M.A. Hasnat, J.H. Lim, Y.M. Lee, E.O. Kim, B.H. Um, B.O. Lim, Preventive and therapeutic effects of blueberry (Vaccinium corymbosum) extract against DSS-induced ulcerative colitis by regulation of antioxidant and inflammatory mediators, J. Nutr. Biochem. 28 (2016) 103–113.

[25] S. Roth, M.R. Spalinger, C. Gottier, L. Biedermann, J. Zeitz, S. Lang, A. Weber, G. Rogler, M. Scharl, Bilberry-derived anthocyanins modulate cytokine expression in the intestine of patients with ulcerative colitis, PLoS One 11 (5) (2016), e0154817.

[26] M. Biagioli, A. Carino, C. Fiorucci, G. Annunziato, S. Marchianò, M. Bordoni, R. Roselli, C.D. Giorgio, F. Castiglione, P. Ricci, A. Bruno, A. Faccini, E. Distrutti, M. Baldoni, G. Costantino, S. Fiorucci, The Aryl Hydrocarbon Receptor (AhR) mediates the counter-regulatory effects of pelargonidins in models of inflammation and metabolic dysfunctions, Nutrients 11 (8) (2019).

[27] M. Biagioli, A. Carino, S. Cipriani, D. Francisci, S. Marchianò, P. Scarpelli, D. Sorcini, A. Zampella, S. Fiorucci, The Bile Acid Receptor GPBAR1 Regulates the M1/M2 phenotype of intestinal macrophages and activation of GPBAR1 Rescues Mice from Murine Colitis, J. Immunol. 199 (2) (2017) 718–733.

[28] A. Carino, S. Cipriani, S. Marchianò, M. Biagioli, C. Santorelli, A. Donini, A. Zampella, M.C. Monti, S. Fiorucci, BAR502, a dual FXR and GPBAR1 agonist, promotes browning of white adipose tissue and reverses liver steatosis and fibrosis, Sci. Rep. 7 (2017) 42801.

[29] U. Erben, C. Loddenkemper, K. Doerfel, S. Spieckermann, D. Haller, M. M. Heimesaat, M. Zeitz, B. Siegmund, A.A. Kühl, A guide to histomorphological evaluation of intestinal inflammation in mouse models, Int. J. Clin. Exp. Pathol. 7 (8) (2014) 4557–4576.

[30] A. Gidari, M. Nofri, L. Saccarelli, S. Bastianelli, S. Sabbatini, S. Bozza, B. Camilloni, I. Fusco-Moffa, C. Monari, E. De Robertis, A. Mencacci, D. Francisci, Is recurrence possible in coronavirus disease 2019 (COVID-19)? Case series and systematic review of literature, Eur. J. Clin. Microbiol. Infect Dis. 40 (1) (2021) 1–12.

[31] E.J. Mendoza, K. Manguiat, H. Wood, M. Drebot, Two detailed plaque assay protocols for the quantification of infectious SARS-CoV-2, Curr. Protoc. Microbiol. 57 (1) (2020) ecpmc105.

[32] D. Wrapp, N. Wang, K.S. Corbett, J.A. Goldsmith, C.L. Hsieh, O. Abiona, B. S. Graham, J.S. McLellan, Cryo-EM structure of the 2019-nCoV spike in the prefusion conformation, Science 367 (6483) (2020) 1260–1263.

[33] C. Toelzer, K. Gupta, S.K.N. Yadav, U. Borucu, A.D. Davidson, M. Kavanagh Williamson, D.K. Shoemark, F. Garzoni, O. Staufer, R. Milligan, J. Capin, A. J. Mulholland, J. Spatz, D. Fitzgerald, I. Berger, C. Schaffitzel, Free fatty acid binding pocket in the locked structure of SARS-CoV-2 spike protein, Science 370 (6517) (2020) 725–730.

[34] G.M. Sastry, M. Adzhigirey, T. Day, R. Annabhimoju, W. Sherman, Protein and ligand preparation: Parameters, protocols, and influence on virtual screening enrichments, J. Comput. Aided Mol. Des. 27 (3) (2013) 221–234.

[35] J.C. Shelley, A. Cholleti, L.L. Frye, J.R. Greenwood, M.R. Timlin, M. Uchimaya, Epik: A software program for pK(a) prediction and protonation state generation for drug-like molecules, J. Comput. Aided Mol. Des. 21 (12) (2007) 681–691.

[36] L. Grippo, S. Lucidi, A globally convergent version of the Polak-Ribière conjugate gradient method, Math. Program. 78 (3) (1997) 375–391.

[37] T.A. Halgren, R.B. Murphy, R.A. Friesner, H.S. Beard, L.L. Frye, W.T. Pollard, J. L. Banks, Glide: A new approach for rapid, accurate docking and scoring. 2. Enrichment factors in database screening, J. Med. Chem. 47 (7) (2004) 1750–1759.

[38] J.L. Banks, H.S. Beard, Y. Cao, A.E. Cho, W. Damm, R. Farid, A.K. Felts, T. A. Halgren, D.T. Mainz, J.R. Maple, R. Murphy, D.M. Philipp, M.P. Repasky, L. Y. Zhang, B.J. Berne, R.A. Friesner, E. Gallicchio, R.M. Levy, Integrated Modeling Program, Applied Chemical Theory (IMPACT), J. Comput. Chem. 26 (16) (2005) 1752–1780.

[39] S. Chiappetta, A.M. Sharma, V. Bottino, C. Stier, COVID-19 and the role of chronic inflammation in patients with obesity, Int. J. Obes (Lond) 44 (8) (2020) 1790–1792.

[40] J.N. McNeill, E.S. Lau, S.M. Paniagua, E.E. Liu, J.K. Wang, I.V. Bassett, C. A. Selvaggi, S.A. Lubitz, A.S. Foulkes, J.E. Ho, The role of obesity in inflammatory markers in COVID-19 patients, Obes. Res. Clin. Pract. (2020).

[41] M. Winter-Jensen, S. Afzal, T. Jess, B.G. Nordestgaard, K.H. Allin, Body mass index and risk of infections: a Mendelian randomization study of 101,447 individuals, Eur. J. Epidemiol. 35 (4) (2020) 347–354.

[42] Y. Zhi, H. Lu, Y. Duan, W. Sun, G. Guan, Q. Dong, C. Yang, Involvement of the nuclear factor-κB signaling pathway in the regulation of CXC chemokine receptor-4 expression in neuroblastoma cells induced by tumor necrosis factor-α, Int. J. Mol. Med. 35 (2) (2015) 349–357.

[43] S. Schütze, K. Wiegmann, T. Machleidt, M. Krönke, TNF-induced activation of NF-kappa B, Immunobiology 193 (2–4) (1995) 193–203.

[44] A. Carino, F. Moraca, B. Fiorillo, S. Marchianò, V. Sepe, M. Biagioli, C. Finamore, S. Bozza, D. Francisci, E. Distrutti, B. Catalanotti, A. Zampella, S. Fiorucci, Hijacking SARS-CoV-2/ACE2 Receptor Interaction by Natural and Semi-synthetic steroidal agents acting on functional pockets on the receptor binding domain, Front. Chem. 8 (2020) 846.

[45] D.K. Shoemark, C.K. Colenso, C. Toelzer, K. Gupta, R.B. Sessions, A.D. Davidson, I. Berger, C. Schaffitzel, J. Spencer, A.J. Mulholland, Molecular simulations suggest vitamins, retinoids and steroids as ligands of the free fatty acid pocket of the SARS-CoV-2 Spike Protein*, Angew. Chem. Int. Ed. Engl. (2021).

[46] A.E. Allam, H.K. Assaf, H.A. Hassan, K. Shimizu, Y.A.M.M. Elshaier, An in silico perception for newly isolated flavonoids from peach fruit as privileged avenue for a countermeasure outbreak of COVID-19, RSC Adv. 10 (50) (2020) 29983–29998.

[47] J.J. Byrnes, S. Gross, C. Ellard, K. Connolly, S. Donahue, D. Picarella, Effects of the ACE2 inhibitor GL1001 on acute dextran sodium sulfate-induced colitis in mice, Inflamm. Res. 58 (11) (2009) 819–827.

[48] J.K. Nowak, J.C. Lindstrøm, R. Kalla, P. Ricanek, J. Halfvarson, J. Satsangi, Age, inflammation, and disease location are critical determinants of intestinal expression of SARS-CoV-2 Receptor, Gastroenterology 159 (3) (2020) 1151–1154. e2.

[49] M.F. Neurath, COVID-19 and immunomodulation in IBD, Gut 69 (7) (2020) 1335–1342.

[50] M.W. Zhuang, Y. Cheng, J. Zhang, X.M. Jiang, L. Wang, J. Deng, P.H. Wang, Increasing host cellular receptor-angiotensin-converting enzyme 2 expression by coronavirus may facilitate 2019-nCoV (or SARS-CoV-2) infection, J. Med. Virol. 92 (11) (2020) 2693–2701.

[51] S. Ding, P.K. Lund, Role of intestinal inflammation as an early event in obesity and insulin resistance, Curr Opin Clin Nutr Metab Care 14 (4) (2011) 328–333.

[52] J.W. Harper, T.L. Zisman, Interaction of obesity and inflammatory bowel disease, World J. Gastroenterol. 22 (35) (2016) 7868–7881.

[53] J. Zhou, C. Li, X. Liu, M.C. Chiu, X. Zhao, D. Wang, Y. Wei, A. Lee, A.J. Zhang, H. Chu, J.P. Cai, C.C. Yip, I.H. Chan, K.K. Wong, O.T. Tsang, K.H. Chan, J.F. Chan, K.K. To, H. Chen, K.Y. Yuen, Infection of bat and human intestinal organoids by SARS-CoV-2, Nat. Med. 26 (7) (2020) 1077–1083.

[54] M.M. Lamers, J. Beumer, J. van der Vaart, K. Knoops, J. Puschhof, T.I. Breugem, R. B.G. Ravelli, J. Paul van Schayck, A.Z. Mykytyn, H.Q. Duimel, E. van Donselaar, S. Riesebosch, H.J.H. Kuijpers, D. Schipper, W.J. van de Wetering, M. de Graaf,

M. Koopmans, E. Cuppen, P.J. Peters, B.L. Haagmans, H. Clevers, SARS-CoV-2 productively infects human gut enterocytes, Science 369 (6499) (2020) 50–54.
[55] M.A. Khajah, M.M. Fateel, K.V. Ananthalakshmi, Y.A. Luqmani, Anti-inflammatory action of angiotensin 1–7 in Experimental Colitis, PLoS One 11 (3) (2016), e0150861.
[56] X.Z. Li, Y. Qiu, L. Jeffery, F. Liu, R. Feng, J.S. He, J.Y. Tan, Z.Y. Ye, S.N. Lin, S. Ghosh, M. Iacucci, M.H. Chen, R. Mao, Down-Regulation of Colonic ACE2 expression in patients with inflammatory bowel disease responding to Anti-TNF Therapy: Implications for COVID-19, Front. Med. (Lausanne) 7 (2020), 613475.
[57] A. Salaritabar, B. Darvishi, F. Hadjiakhoondi, A. Manayi, A. Sureda, S.F. Nabavi, L. R. Fitzpatrick, S.M. Nabavi, A. Bishayee, Therapeutic potential of flavonoids in inflammatory bowel disease: A comprehensive review, World J. Gastroenterol. 23 (28) (2017) 5097–5114.
[58] K. Venkatakrishnan, H.F. Chiu, C.K. Wang, Extensive review of popular functional foods and nutraceuticals against obesity and its related complications with a special focus on randomized clinical trials, Food Funct. 10 (5) (2019) 2313–2329.
[59] J. Øvrevik, M. Låg, V. Lecureur, D. Gilot, D. Lagadic-Gossmann, M. Refsnes, P. E. Schwarze, T. Skuland, R. Becher, J.A. Holme, AhR and Arnt differentially regulate NF-κB signaling and chemokine responses in human bronchial epithelial cells, Cell Commun Signal 12 (2014) 48.
[60] C.F. Vogel, F. Matsumura, A new cross-talk between the aryl hydrocarbon receptor and RelB, a member of the NF-kappaB family, Biochem. Pharmacol. 77 (4) (2009) 734–745.